Influence of quantum confinement and strain on orbital polarization of four-layer LaNiO_{3} superlattices: A DFT+DMFT study

Hyowon Park, Andrew J. Millis, and Chris A. Marianetti

Phys. Rev. B **93**, 235109 — Published 7 June 2016

DOI: 10.1103/PhysRevB.93.235109

Influence of quantum confinement and strain on orbital polarization of four-layer $LaNiO_3$ superlattices: a DFT+DMFT study

Hyowon Park,[1,2] Andrew J. Millis,[3] and Chris A. Marianetti[4]

[1] *Department of Physics, University of Illinois at Chicago, Chicago, Illinois 60607, USA*
[2] *Materials Science Division, Argonne National Laboratory, Argonne, Illinois 60439, USA*
[3] *Department of Physics, Columbia University, New York, NY 10027, USA*
[4] *Department of Applied Physics and Applied Mathematics, Columbia University, New York, NY 10027, USA*

(Dated: May 23, 2016)

Atomically precise superlattices involving transition metal oxides provide a unique opportunity to engineer correlated electron physics using strain (modulated by choice of substrate) and quantum confinement (controlled by layer thickness). Here we use the combination of density functional theory and dynamical mean field theory (DFT+DMFT) to study Ni E_g d-orbital polarization in strained $LaNiO_3/LaAlO_3$ superlattices consisting of four layers of nominally metallic NiO_2 and four layers of insulating AlO_2 separated by LaO layers. The layer-resolved orbital polarization is calculated as a function of strain and analyzed in terms of structural, quantum confinement, and correlation effects. The effect of strain is determined from the dependence of the results on the Ni-O bond-length ratio and the octahedral rotation angles; quantum confinement is studied by comparison to bulk calculations with similar degrees of strain; correlation effects are inferred by varying interaction parameters within our DFT+DMFT calculations. The calculated dependence of orbital polarization on strain in superlattices is qualitatively consistent with recent X-ray absorption spectroscopy and resonant reflectometry data. However, interesting differences of detail are found between theory and experiment. Under tensile strain, the two inequivalent Ni ions display orbital polarization similar to that calculated for strained bulk $LaNiO_3$ and observed in experiment. Compressive strain produces a larger dependence of orbital polarization on Ni position and even the inner Ni layer exhibits orbital polarization different from that calculated for strained bulk $LaNiO_3$.

I. INTRODUCTION

Much of the interesting physics of transition metal oxides arises from the unusual properties of strongly interacting electrons in partly occupied transition metal d-shells. A key property of a partly filled d-shell is orbital polarization, the relative occupancy of different d-levels[1]. Interest in the possibility of using "orbital engineering" to control orbital polarization and thereby obtain desired electronic properties continues to grow given the improving capability of synthesizing atomic-scale superlattices involving transition metal oxides[2,3]. Superlattices allow for metastable structures with a range of lattice strain and many permutations of layerings, most of which could not be achieved by standard bulk crystal growth methods. Much attention has focused on superlattice systems based on rare earth nickelates following the theoretical prediction[4,5] that complete orbital polarization of one of the Ni d-multiplets might be realized in superlattices composed of alternating layers of $LaNiO_3$ and an insulating spacer layer and that the cuprate-like band structure implied by the complete orbital polarization might lead to high T_c superconductivity in the superlattice. More advanced DFT+DMFT calculations later suggested that this scenario will not be realized[6], and this theoretical prediction is consistent with current experimental observations[7].

Measuring orbital polarization is challenging, especially in artificially synthesized superlattices where the small volumes of typical samples mean that many types of experiments are not practicable. However recent experimental progress in x-ray absorption and resonant reflectivity measurements have provided very interesting information[7–9]. Connecting these experiments to theory to achieve a comprehensive understanding of the factors involved in controlling the orbital physics is an important task.

Theoretical studies of orbital polarization in nickelate heterostructures and films have appeared. Methods used include model system calculations, density functional theory (DFT), DFT+U, and the combination of DFT and the GW approximation. Most studies however have used the combination of density functional theory and dynamical mean field theory (DFT+DMFT). Effects that have been analyzed include quantum confinement[4–6,10,11], strain[5,6,10–13], local chemistry[12], and the consequences of charge doping[14,15].

The energy window used to define the correlated orbitals is an important issue in beyond DFT calculations such as the DFT+DMFT methodology[16]. The general consensus is that for the rare earth nickelates the correlated subspace should be defined in terms of atomic-like d-orbitals defined using Wannier or projector techniques applied to a wide energy range spanning at least the full $p-d$ manifold[6] (this is also the choice made in standard DFT+U implementations). As noted by Peil et al[13], if one wishes instead to define the correlated manifold in terms of the near Fermi-surface $p-d$ antibonding bands, the interaction parameters must be strongly renormalized.

A key finding of the published theoretical work is that the Hunds coupling acts to suppress orbital polarization down to a level substantially below the value predicted by standard DFT[6,13]. However, DFT+U calculations in bulk $LuNiO_3$ demonstrated that a Jahn-Teller distorted structure is only slightly higher in energy[17] than the bond disproportionated ground state, and a sufficiently large ($\gtrsim 4\%$) tensile (cubic-tetragonal with the in-plane bonds being longer) strain stabilizes the Jahn-Teller distorted structure[18]. The effect of more modest tensile strain on the Ni-O bond-length ratio and the octahedral rotation was studied for tensile-strained bulk $LaNiO_3$[13], and the calculated orbital polarization was found to be in good agreement with the X-ray experiment[13].

This paper is motivated by recent tour-de-force measurements[7,9] of orbital polarization of the two inequivalent Ni sites (ie. inner and outer Ni-sites) in $(LaNiO_3)_4/(RXO_3)_4$ superlattices comprised of alternating layers of four unit cells of $LaNiO_3$ and four unit cells of an insulating spacer layer RXO_3 with R=La,Dy,Gd and X=Al,Ga,Sc. By varying R and X, the in-plane lattice constant could be adjusted to provide either tensile or compressive biaxial strain on the $LaNiO_3$ material while differences between orbital polarization of the Ni ion adjacent to the RXO_3 and orbital polarization of the Ni ion surrounded by other Ni ions provides some insight into chemical and quantum confinement contributions.

We build on the previously introduced theoretical techniques to ask the question: can a state of the art DFT+DMFT calculation based on a realistic crystal structure account for the essential features of the experiment? We study $(LaNiO_3)_4/(LaAlO_3)_4$ superlattices with four NiO_2 layers alternating with four AlO_2 layers. We incorporate the effects of strain (implemented in the experiment by changing the $LaAlO_3$ to other wide gap perovskite insulators) by fixing the in-plane lattice constant. We compare the DFT+DMFT calculations to pure DFT calculations and within the DFT+DMFT calculations consider different values of the correlation parameters. We estimate quantum confinement effects by comparing our results to those obtained on strained bulk $LaNiO_3$.

The rest of this paper is organized as follows. In Section II we present the specifics of the calculations. In Section III we present our calculated orbital polarization and in Section IV we show the one-particle spectra. In Section V we discuss the impact of structure and quantum confinement on orbital polarization and in Section VI we delineate the consequences of the many-body interactions. Section VII is conclusion.

II. MODEL AND METHODS

We study superlattices consisting of four layers of $LaNiO_3$ alternating with four layers of the wide bandgap insulator $LaAlO_3$ with the alteration along the (001) direction of the ideal cubic perovskite structure; we refer to the resulting structures as (001) $(LaNiO_3)_4/(LaAlO_3)_4$ superlattices. We impose tetragonal symmetry, meaning that the two in-plane lattice constants a are equal and the lattice vectors are at right angles to each other and to the out-of-plane lattice vector. We allow for rotations and tilts of the NiO_6 and AlO_6 octahedra; this doubles the unit cell in-plane though the combination of an in-plane translation and a rotation maps one NiO_6 octahedron onto the other. The four $LaNiO_3$ layers come in two equivalent pairs. We denote the Ni in the outer (closer to Al) layer as Ni B and the Ni in the inner layer as Ni A.

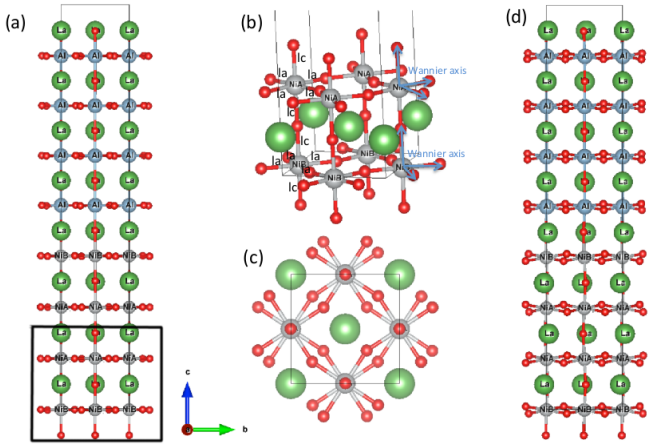

Figure 1. (Color online) (a) The crystal structure of $(LaNiO_3)_4/(LaAlO_3)_4$ superlattice at compressive (-3.1%) strain. La (green), Ni (grey), Al (blue), O (red) atoms are shown. Both the inner-layer Ni (Ni A) and the outer-layer Ni (Ni B) are also denoted. The two Ni (A and B) layers (enclosed by a black rectangle) are zoomed in at (b) and (c). (b) The zoom-in structure of the two Ni layers. Here, l_c denotes the out-of-plane Ni-O bond-length and l_a means the in-plane Ni-O bond-length. The blue arrows indicate the local coordinates of Wannier orbitals used in DFT+DMFT calculations. The local axis almost coincides with the Ni-O bonding axis. (c) The top-view of the two Ni layers (enclosed by a black rectangle) in (a) showing the octahedral rotation about the normal axis. (d) The crystal structure of $(LaNiO_3)_4/(LaAlO_3)_4$ superlattice at tensile (2.6%) strain. All structure figures are generated using the VESTA program[19].

We simulate strain by varying the in-plane lattice constant and define tensile (compressive) strain as in-plane lattice constant larger (smaller) than the mean Ni-Ni distance a_0 calculated for bulk $LaNiO_3$; quantitatively, (in-plane) strain is $(a-a_0)/a_0$. The theoretical a_0 value obtained by performing a structural relaxation within the GGA methodology is 3.87Å and the measured equilibrium volume used to define strain in the experiment is 3.838Å[7].

In the first step in our calculations we use DFT to relax all internal coordinates and the (001) axis lattice parameter under the assumption of tetragonal symmetry and fixed strain, meaning that the in-plane lattice constants are fixed at definite values and constrained to

be at right angles. (We thus neglect the small monoclinic distortion occurring in bulk $LaNiO_3$; the effects of this distortion are considered in Ref. 13.) The structural relaxation of atomic positions is performed using the Vienna Ab-initio Simulation Package (VASP)[20,21], a plane-wave DFT code based on the projector augmented wave formalism[22]. The exchange-correlation potential is taken to be the spin-polarized generalized gradient approximation (s-GGA) using the Perdew-Burke-Ernzerhof (PBE) functional[23] and in our calculations the ground state is ferromagnetic. GGA is used for relaxations as opposed to GGA+DMFT due to the massive savings in computational cost, in addition to current technical constraints for computing forces. The structural relaxation is converged if the atomic forces of all atoms are smaller than 0.01eV/Å. We note that for physically relevant $U \gtrsim 5eV$, DFT+U relaxation calculations based on spin-polarized GGA or non-spin-polarized GGA wrongly produce the bond disproportionated structure for $LaNiO_3$ even at ambient pressure[16,24]. A $k-$point mesh of $8\times8\times1$ is used and the plane-wave energy cutoff E_{cut} is set to be 600eV. Note that only one k_z point is sufficient as the supercell is enormously elongated in the $z-$direction; we confirmed (not shown) that a $8\times8\times2$ $k-$mesh relaxes to an essentially identical structure ($\sim 0.1\%$ changes to octahedral l_c/l_a ratio (see definition in Fig. 5 caption) and $\sim 1\%$ changes to rotation angles).

We specify the rotation patterns for given structure using Glazer notation[25,26]. Experimentally, bulk $LaNiO_3$ has a rhombohedral unit cell (space group $R\bar{3}c$, Ref. 27) with the NiO_6 octahedral rotation of the $a^-a^-a^-$ pattern. The $a^-a^-c^+$ pattern is also observed for nickelates with a smaller rare-earth ion than La[28]. In our calculations, for strained bulk $LaNiO_3$ on a cubic substrate we find the $a^-a^-c^-$ pattern. Our strained $LaNiO_3$ superlattice shows asymmetric behavior depending on the sign of strain. Under compressive strain the relaxed structure exhibits the $a^-a^-c^-$ pattern of the NiO_6 octahedral rotation similar to strained bulk while the $a^-a^-c^+$ pattern becomes stable under tensile strain.

For each relaxed structure we use the generalized gradient approximation plus dynamical mean field theory (GGA+DMFT) to calculate the electronic structure. In these calculations we use the spin-unpolarized form of the GGA-PBE functional and constrain the DMFT calculations to the paramagnetic phase; this is appropriate since no magnetism has been observed in the system of experimental interest[7,29,30]. The correlated subspace is taken to be the atomic-like Ni d-orbitals defined by a standard maximally localized Wannier function construction[31] based on a wide energy window spanning the full 12eV energy range of the Ni-3d O-2p band complex. We follow previous work [16,17,24] and rotate the orbital quantization axis on each Ni site to the direction that minimizes the off diagonal components of the local Hamiltonian within each Ni subspace. As a result, the off diagonal components of the hybridization function are also minimized. This direction is approximately aligned to the local Ni-O octahedral axes (see Fig 1 (b) for these quantization axis). The filled t_{2g} orbitals are treated using a Hartree-Fock approximation while the full dynamics of the e_g orbitals is considered, as in our previous studies[16,17,24]. We have used the continuous-time quantum Monte Carlo impurity solver[32,33] and only the diagonal hybridization function is kept during the Monte Carlo run for an efficient sampling.

We adopt rotationally invariant Slater-Kanamori interactions within the Ni d correlated subspace. The interactions are parametrized by a Coulomb repulsion U, a Hunds coupling J and a double counting correction U'. Therefore, the multi-orbital Hamiltonian treated in this paper is given by

$$\begin{aligned}\hat{H} = & U\sum_{i,\alpha}\hat{n}_{i\alpha\uparrow}\hat{n}_{i\alpha\downarrow} + (U-2J)\sum_{i,\alpha\neq\beta}\hat{n}_{i\alpha\uparrow}\hat{n}_{i\beta\downarrow} \\ & +(U-3J)\sum_{i,\alpha>\beta,\sigma}\hat{n}_{i\alpha\sigma}\hat{n}_{i\beta\sigma} \\ & +J\sum_{i,\alpha\neq\beta}\left(\hat{\psi}^\dagger_{i\alpha\uparrow}\hat{\psi}_{i\beta\uparrow}\hat{\psi}^\dagger_{i\beta\downarrow}\hat{\psi}_{i\alpha\downarrow} + \hat{\psi}^\dagger_{i\alpha\uparrow}\hat{\psi}_{i\beta\uparrow}\hat{\psi}^\dagger_{i\alpha\downarrow}\hat{\psi}_{i\beta\downarrow}\right)\end{aligned} \tag{1}$$

where i is the Ni atom index, α is the d orbital index, and σ is the spin. The details of solving the above Hamiltonian within DMFT are explained in our previous paper[16]. Our previous work[16,24] showed that U=5eV, $U'=4.8$eV and J=1eV provided the best fit to the structural and metal insulator phase diagram across the rare-earth nickelate family. In this paper we use these values but consider $J=0.7$eV as well as $J=1.0$eV to provide insight into the J-dependence, since the value of J was previously shown to be important for the quantitative value of orbital polarization.[6,13]

The main quantity of interest in this paper is orbital polarization, P. A precise definition is required, since the values obtained depend on the way the d-orbitals and polarization are defined. Here we adopt the defintion of P used in Ref.7, with the d-orbitals defined as the rotated Wannier orbitals $|W^a_{e_g}\rangle$ discussed above and $a=3z^2-r^2$ or x^2-y^2 denoting the e_g orbitals of main interest here. The orbital occupancies are then the diagonal elements of the occupancy matrix

$$n^{aa}_{e_g} = \frac{T}{N_{\mathbf{k}}}\sum_{i\omega_n,\mathbf{k}}\sum_{(l,l')\in w}\langle W^a_{e_g}|\psi_{\mathbf{k}l}\rangle G^{\mathbf{k}}_{ll'}(i\omega_n)\langle\psi_{\mathbf{k}l'}|W^a_{e_g}\rangle, \tag{2}$$

$$\hat{G}^{\mathbf{k}}(i\omega_n) = \frac{1}{(i\omega_n+\mu)\hat{\mathbb{I}} - \hat{H}^{KS}_{\mathbf{k}} - \hat{P}^\dagger_{cor}\cdot\hat{\Sigma}_d(i\omega_n)\cdot\hat{P}_{cor}} \tag{3}$$

where $\hat{H}^{KS}_{\mathbf{k}}$ is the Kohn-Sham Hamiltonian at the $\mathbf{k}$ point in the Brillouin zone, $\psi_{\mathbf{k}l}$ is the corresponding Kohn-Sham eigenfunction with band index l, Σ_d is the self energy for the Wannier d orbitals, and $\hat{P}_{cor}$ is a projection operator defined to downfold to the correlated d

subspace. ω_n is the Matsubara frequency and T is the temperature. Within GGA, $n_{e_g}^{aa}$ is obtained by inserting $\Sigma_d = 0$.

Orbital polarization P is then defined in terms of the hole density per spin $h^a = 1 - n_{eg}^{aa}$ as

$$P = \left(\frac{4}{n_{e_g}^{atomic}} - 1 \right) \frac{(X-1)}{(X+1)} \tag{4}$$

with $X = h^{3z^2-r^2}/h^{x^2-y^2}$ and $n_{e_g}^{atomic}$ is the occupation value for the atomic-like Wannier function which we set to 1.0 for consistency with Ref. 7. Thus positive P means the lower relative occupancy of the $3z^2 - r^2$ orbital.

III. RESULTS: ORBITAL POLARIZATION

Fig. 2 shows our main results: orbital polarization P computed for the superlattice and for bulk $LaNiO_3$ and compared to experimental data. Our results for bulk $LaNiO_3$ (panel c) are very similar to those presented by Peil *et al* [13]. The GGA results agree almost exactly under both tensile and compressive strain. The GGA+DMFT results are consistent given the difference in parameters (Peil *et al* considered U=8eV and J=1eV whereas we consider U=5eV and J=0.7eV; the increase in polarization due to the increase in U is almost compensated by the decrease in polarization due to the increase in J. The close correspondence of our DFT and DFT+DMFT (allowing for differences in U) results to those of Peil *et al* shows that our neglect of the monoclinic distortion is justified.

We see that both the GGA and the GGA+DMFT calculations for superlattices (panel a and b) are in reasonable qualitative correspondence with experiment both in terms of the order of magnitude of the change over the interesting strain range and in terms of the sign of the difference between polarizations of the inner and outer Ni layers. Consistent with experiment, all calculations indicate that tensile strain increases orbital polarization (relative occupancy of $d_{3z^2-r^2}$ orbital) while compressive strain decreases it. Also consistent with experiment, the calculations indicate that at any value of the strain orbital polarization of the A (inner layer) site is less than that of the B (outer layer) site, meaning that the inner layer Ni ion has lower occupancy of the $x^2 - y^2$ and higher occupancy of the $3z^2 - r^2$ orbital than does the outer layer Ni ion.

The observed change of P with strain in the bulk material (Fig. 2c) may be qualitatively understood as a consequence of the antibonding nature of the near Fermi surface bands. Considering for example tensile strain, the increase in l_a reduces the hybridization of the planar Ni orbital to the surrounding oxygens, thus lowering the energy of the $x^2 - y^2$ derived band, decreasing the density of $x^2 - y^2$ holes, while the concomitant decrease in l_c conversely increases the hybridization to the $3z^2 - r^2$ orbital, increasing the density of $3z^2 - r^2$ holes.

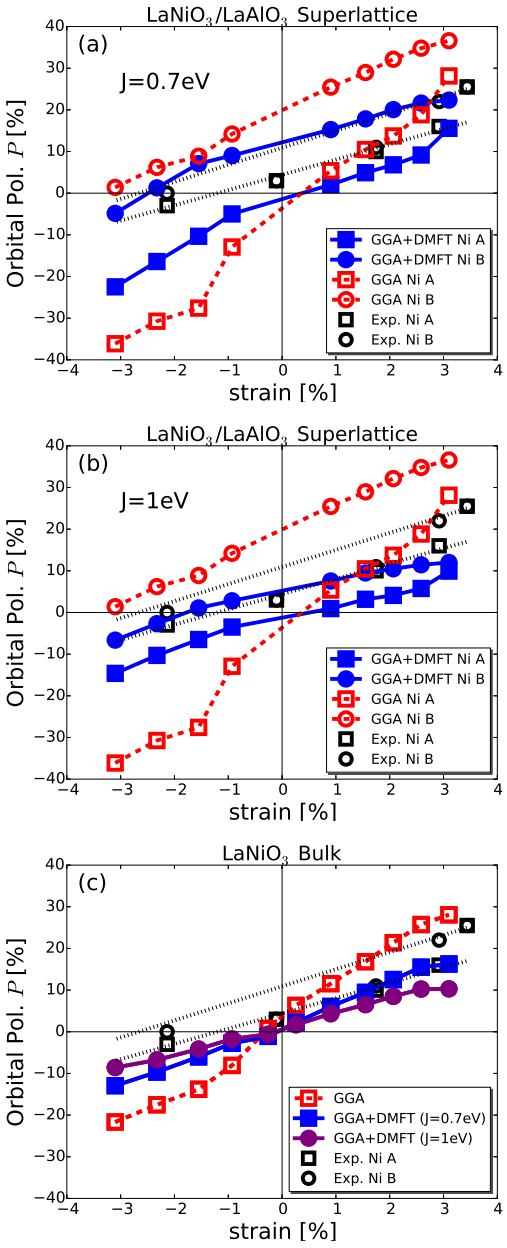

Figure 2. (Color online) Orbital polarization P (Eq. 4) as a function of bi-axial strain for the two inequivalent Ni sites of the 4/4 $LaNiO_3/LaAlO_3$ superlattice (panels a and b) and for strained bulk $LaNiO_3$ (panel c) computed using paramagnetic GGA+DMFT. Interaction parameters of U=5eV and J=0.7eV (panel a), U=5eV and J=1eV (panel b), and $U = 5$ eV and J=0.7/1.0eV (panel c) are used. Paramagnetic pure GGA results are also presented, as are experimental data (black empty dots, dashed lines) obtained from Ref. 7.

While all of the calculations are qualitatively consistent, interesting quantitative differences occur. The GGA calculations predict a stronger dependence of orbital polarization on strain and on Ni site, and predict a stronger change across zero strain, than do the GGA+DMFT calculations, with the difference between

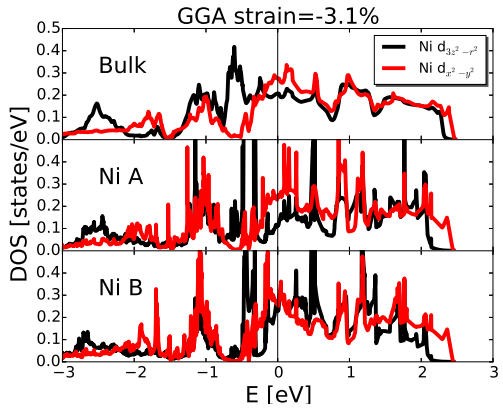

Figure 3. (Color online) The d-orbital resolved density of states (DOS) computed within GGA for bulk $LaNiO_3$ (Top panel), and $LaNiO_3/LaAlO_3$ superlattice Ni A (Middle panel) and Ni B (Bottom panel). The compressive strain (-3.1%) is applied for both bulk and superlattice. The black line denotes the $d_{3z^2-r^2}$ orbital and the red line represents the $d_{x^2-y^2}$ orbital.

GGA and GGA+DMFT being larger for larger J. This is an example of the physics discussed in Ref. 6: the electronic configuration of the Ni atoms is closer to $d^8\bar{L}$ than to d^7 so as Hunds coupling is increased the probability that the Ni is in the high spin d^8 state increases, and in the high-spin d^8 state both e_g orbitals are occupied so orbital polarization is suppressed. However, as we shall show below the details of the J-dependence of different aspects of the strain dependence is somewhat unexpected.

IV. RESULTS: THE ONE-PARTICLE SPECTRA

Orbital polarization P is directly related to the change of the d-orbital resolved one-particle Green's function (Eq. 2). In this section, we show the d-orbital resolved density of states (DOS) computed for the $LaNiO_3/LaAlO_3$ superlattices. First Fig. 3 displays the DOS computed within GGA for the $LaNiO_3/LaAlO_3$ superlattice (Ni A: Middle panel, Ni B: Bottom panel), also compared to the bulk $LaNiO_3$ case (Top panel). The most compressive strain (-3.1%) case is shown for both bulk and superlattice structures. Both the $d_{3z^2-r^2}$ orbital (the black line) and the $d_{x^2-y^2}$ orbital (the red line) are depicted. Under the compressive strain, the $d_{x^2-y^2}$ orbital is strongly hybridized with O p orbitals and as a result the $d_{x^2-y^2}$ hole density is more enhanced than the $d_{3z^2-r^2}$ hole density as shown in the bulk DOS (Fig. 3 top). The superlattice DOS (middle and bottom panels) shows a relatively narrow bandwidth (specially for the $d_{3z^2-r^2}$ orbital) compared to the bulk and the spectra exhibit a spiky feature due to the large unit cell. The $d_{x^2-y^2}$ DOS is rather similar regarding both Ni A (middle panel) and Ni B (bottom panel) layers and also compared to the bulk $d_{x^2-y^2}$ DOS. However, $d_{3z^2-r^2}$ DOS varies noticeably between Ni A and Ni B layers showing the enhanced (reduced) hole density for the Ni B (Ni A) layer compared to the bulk. We attribute this result to the structural and the quantum confinement effects as will be shown in the next section.

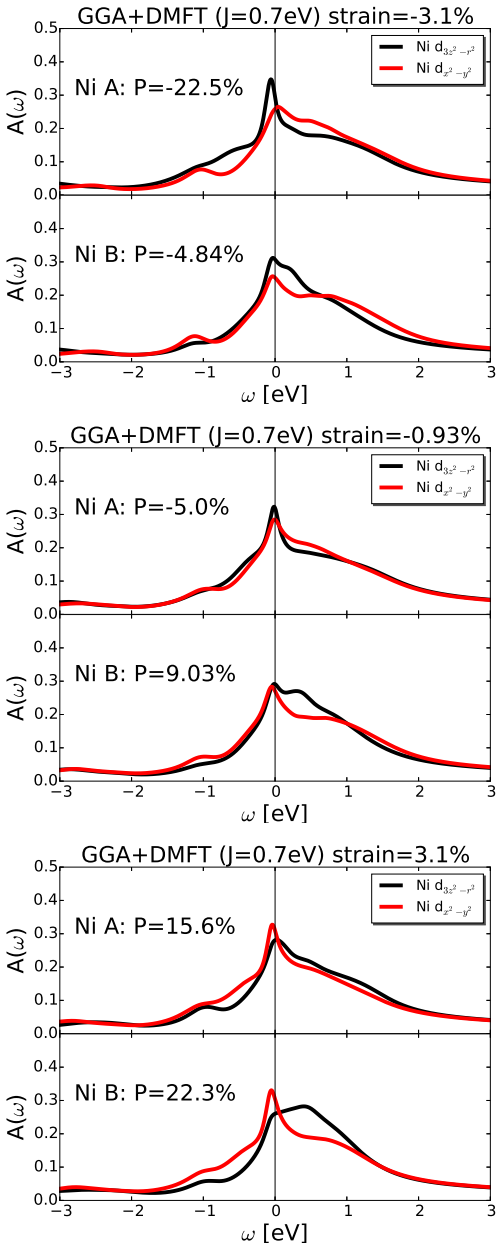

Figure 4. (Color online) The d-orbital resolved one-particle spectra $A(\omega)$ (in the units of states/eV) computed within GGA+DMFT (U=5eV and J=0.7eV) for $LaNiO_3/LaAlO_3$ superlattices. Different strain results for -3.1% (top figure), -0.93% (middle figure), and 3.1% (bottom figure) are shown. Both Ni A (top panel) and Ni B (bottom panel) results are displayed for each figure. The black line denotes the $d_{3z^2-r^2}$ orbital and the red line represents the $d_{x^2-y^2}$ orbital.

Fig. 4 shows the d-orbital resolved one-particle spec-

tra $A(\omega)$ computed within GGA+DMFT for the $LaNiO_3/LaAlO_3$ superlattice (Ni A: top panel, Ni B: bottom panel). The strain effect is imposed from the most compressive (-3.1% (top figure)) strain, the near-zero (-0.93% (middle figure)) strain, and to the most tensile (3.1% (bottom figure)) strain. Compared to the bare GGA DOS, the GGA+DMFT spectra show the renormalization effect near the Fermi energy ($\omega = 0$) and also broad Hubbard bands at higher energies. One should note that GGA+DMFT spectra ($E = E_F$) at -3.1% strain (Fig. 4 top figure) does not correspond to the GGA DOS ($E = E_F$) at the same strain (Fig. 3) since the real part of the self energy effectively shifts the band structure (see Fig. 9). As the strain changes from compressive to tensile, the $d_{3z^2-r^2}$ hole density increases for both Ni A and B layers as expected from the enhanced hybridization effect. And the outer Ni B layer exhibits the higher hole density compared to the inner Ni A layer, consistent with the orbital polarization data.

V. ANALYSIS: STRUCTURAL EFFECTS

In this section we analyze the relation between the structural distortions induced by strain and orbital polarization. We begin with Fig. 5 which shows the calculated strain dependence of the octahedral distortion l_c/l_a (ratio of apical to in-plane Ni-O bond lengths). The dashed line with open symbols shows that for bulk $LaNiO_3$, as expected, an increase in the planar bond length (tensile strain) leads to a decrease in the c-axis bond length, and conversely. The slope of the l_c/l_a curve implies that the bulk material has a calculated Poisson ratio $\nu = -(\delta l_c/\delta l_a)/(2 - \delta l_c/\delta l_a)$ of roughly 0.25 ($\delta l_c/\delta l_a = \delta(l_c/l_a)/\delta(\epsilon_x) + 1$ where ϵ_x is the strain in the x-direction and note that the octahedral bond lengths do not correspond exactly to changes in lattice constants because the octahedral rotations also vary).

A small anomaly in the l_c/l_a ratio occurs at slightly compressive strain (-1%). This arises from an abrupt change in the octahedral rotation angle occurring at this strain, shown in Fig. 6. Near zero strain, the strain effect is accommodated by the octahedral rotation rather than the octahedral distortion. The orientations are specified by rotation angle γ about the axis normal to the plane which is stressed and α about an axis lying in the stress plane. Consistent with experimental data[34], for compressive strain the calculations indicate the dominant rotation is around the z axis and the rotation about the in-plane axis is small ($\gamma \gg \alpha \sim 0$), while for tensile strain the rotation about the in-plane axis is large and there is no rotation about the axis normal to the stress plane.

To obtain a more quantitative and precise understanding of the relation between structure and polarization we replot the data in Fig. 2c in terms of octahedral distortion d defined as

$$d = 1 - \frac{l_c}{l_a} \tag{5}$$

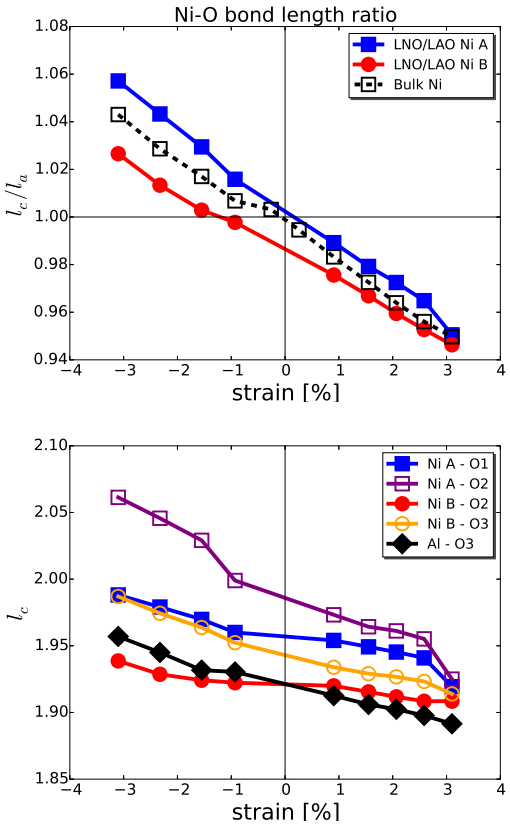

Figure 5. (Color online) Top panel: The layer-resolved Ni-O bond length ratio l_c/l_a (l_c: out-of-plane bond length, averaged over the two out of plane bonds for a given Ni, l_a: in-plane bond length, averaged over the four in plane bonds for a given Ni) for Ni A and Ni B sites as a function of strain for 4/4 $LaNiO_3/LaAlO_3$ superlattice (filled dots, solid line) and bulk $LaNiO_3$ (empty dots, dashed line) Bottom panel: The layer-resolved out-of-plane Ni-O and Al-O bond lengths l_c. O1 denotes the apical O layer between two Ni A layers, i.e. the middle layer of the Ni-O superlattice layers. O2 means the O layer between Ni A and Ni B layers. O3 denotes the O layer between Ni B and Al layers.

Results are shown as dashed-dot (GGA), solid (DMFT J=0.7eV), and dashed (DMFT J=1eV) lines in Fig. 7. We find that the dependence of P on distortion is approximately linear and may be written as

$$P(d) = P_0 + Rd \tag{6}$$

The slope R defines the response of orbital polarization to an E_g-symmetry octahedral distortion, in other words the degree to which a distortion of a Ni-O octahedron leads to a differential occupancy of the Ni e_g levels. The intercept P_0 gives a measure of the other contributions to orbital polarization; in the bulk case, the only other contribution comes from the octahedral rotations, while in the superlattices quantum confinement effects may also play a role.

Results for P_0 and R are given in Table I. We see that for the bulk material, the difference of P_0 values between

between positive and negative d is small, of the order of $10-20\%$ of the total change in P across the strain range we study, and the difference in R is also not large. However, the slope R is strongly increased across the unstrained point and the P_0 value is almost zero (Fig. 7). We interpret these changes as arising from the abrupt change in octahedral rotations across this point. In agreement with previous work[6,13], we find that many-body effects, in particular increasing the Hunds coupling J, act to decrease both the magnitude of P and its response to structural change R. It is interesting to note that the interactions decrease P_0 by a relatively larger amount than they reduce R and that the renormalization of R is larger for tensile strain. We will discuss the reason in section VI.

We now turn to the superlattice. Here the physics is richer. Fig. 2 shows a pronounced difference in polarization between A and B Ni ions, much larger changes across zero strain, and much greater variation of slopes. From Fig. 5 we see also a greater richness of structural effects. The Ni-A and Ni-B sites respond differently to strain: the distortion of the inner (Ni A) octahedron is greater than the distortion of the outer (Ni B) octahedron with the A-B difference being greatest for compressive strain and becoming very small for large tensile strain. The difference of the Ni-O bond length l_c between two apical O ions becomes also greatest for compressive strain and smallest for tensile strain, accounting for this distinct response of l_c/l_a under the sign change of the strain (see Fig. 5 bottom panel).

The primary reason for the difference in distortion is that the bonding between the apical O and the Al is weaker than the bonding between the apical O and the Ni B. Under compressive strain, the Al layer in effect provides a steric hindrance which prevents the O from coming too close to the Al, thus inhibiting the elongation of the Ni B-apical O bond length favored by compressive strain while the Ni A-apical O bond length is greatly elongated. Under tensile strain, a shorter Ni-apical O bond length is preferred, but the energy cost for increasing the Al-O bond length from its preferred value is much less than the cost of decreasing it, thus explaining the near equivalence of the structural distortions of the Ni-A and Ni-B under tensile strain.

The octahedral rotations are also different for tensile and compressive strain. The rotation pattern for the NiO_6 octahedra itself changes from the $a^-a^-c^-$ pattern observed at all strains in bulk and for compressive strain in the superlattice to $a^-a^-c^+$ for tensile strain. (The rotation pattern found for the AlO_6 octahedra is always $a^-a^-c^-$). Fig. 8 shows that for compressive strain the dominant rotation is around the z axis and the out of plane rotation is negligible $\gamma \gg \alpha \sim 0$ as is the case for the bulk materials. However, for tensile strain both rotations occur, with rotations around the in-plane somewhat larger but rotations about the z axis are not negligible. The non-negligible α found for tensile strain arises from a transverse motion of the oxygen which makes it easier for the system to reach a compromise between the preferred Al-O and Ni-O in-plane bond lengths. With this information in hand we turn to the dependence of orbital

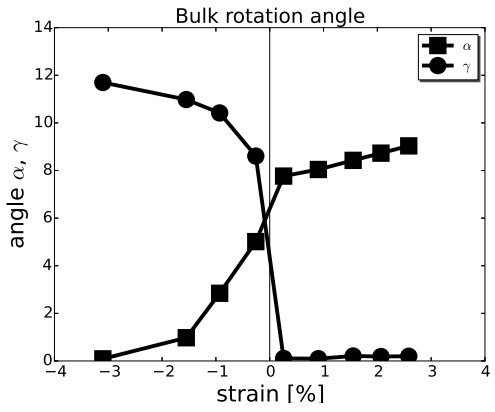

Figure 6. (Color online) Strain dependence of octahedral rotation angles γ (about axis normal to the stress plane) and α (about axis lying in the stress plane) for bulk $LaNiO_3$.

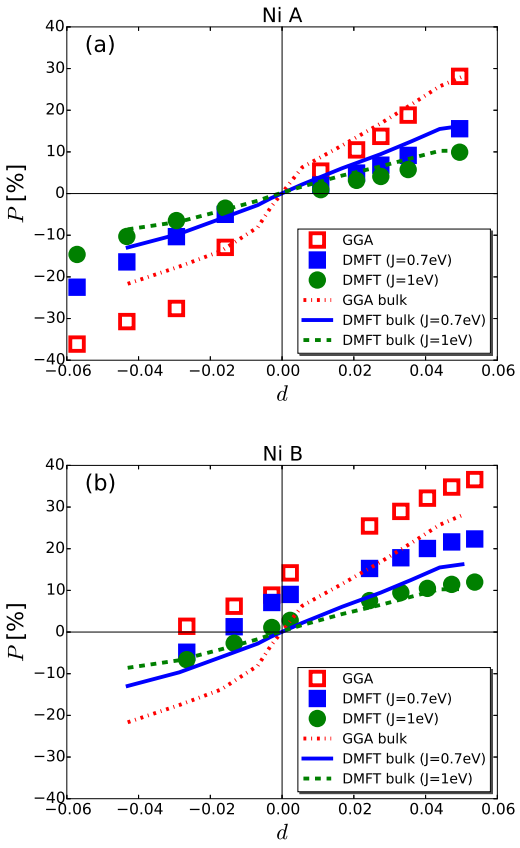

Figure 7. (Color online) Orbital polarization as a function of octahedral distortion $d = 1 - \frac{l_c}{l_a}$ computed using GGA and GGA+DMFT (J=0.7 and 1.0 eV) for the (a) Ni A and (b) Ni B sites of the 4/4 $LaNiO_3/LaAlO_3$ superlattice (points) compared to results for strained bulk $LaNiO_3$ (lines).

Bulk	Compressive	Tensile
P_o GGA	-6.6	2.7
P_o DMFT (J=0.7 eV)	-1.1	0.12
P_o DMFT (J=1.0 eV)	-0.75	0.61
R GGA	3.6	5.2
R DMFT (J=0.7 eV)	2.8	3.5
R DMFT (J=1.0 eV)	1.9	2.2

Ni A Site	Compressive	Tensile
P_o GGA	-18	-0.71
P_o DMFT (J=0.7 eV)	2.6	-1.1
P_o DMFT (J=1.0 eV)	2.2	-1.1
R GGA	3.1	5.4
R DMFT (J=0.7 eV)	4.4	2.9
R DMFT (J=1.0 eV)	2.9	1.9

Ni B Site	Compressive	Tensile
P_o GGA	12	15
P_o DMFT (J=0.7 eV)	8.1	8.5
P_o DMFT (J=1.0 eV)	2.0	3.7
R GGA	4.1	4.1
R DMFT (J=0.7 eV)	4.9	2.8
R DMFT (J=1.0 eV)	3.3	1.7

Table I. Parameters P_0 and R of Eq. 6 resulting in the best linear fit to orbital polarization as a function of octahedral distortion d for each Ni site and bulk. GGA and GGA+DMFT with J=0.7 and 1 eV are compared.

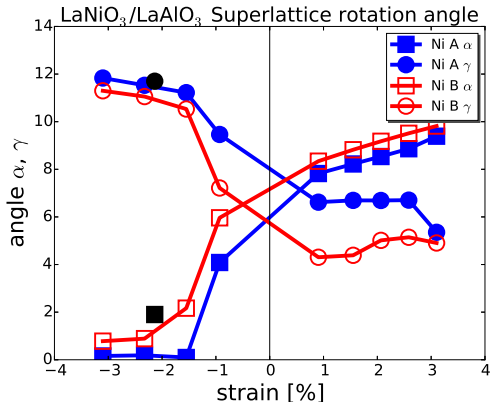

Figure 8. (Color online) The layer-resolved NiO_6 octahedral rotational angles: α, out-of-plane rotation around x axis, (square dots) and γ, in-plane rotation around z axis (circular dots) for 4/4 $LaNiO_3/LaAlO_3$ superlattices. Ni A (filled dots) and Ni B (empty dots) are shown. The black dots under compressive strain denote experimental values obtained for 4/4 $LaNiO_3/LaAlO_3$[35].

polarization on octahedral distortion shown in Fig. 7. For the Ni-A site (panel a) both the superlattice orbital polarization P (points) and the dependence of P on the octahedral distortion (R) under tensile strain are very similar to that found for the bulk materials (lines); however for compressive strain the absolute P values in the superlattice are rather larger than bulk while the effect of interactions (DMFT) is to strongly reduce P toward bulk values. The DMFT effect on the slope R under compressive strain is smaller and indeed of opposite sign, leading for $J = 0.7$eV to a slightly larger R than in GGA.

The most important effect apparent in the Ni-B site results (Fig. 7 (b)) is a large positive offset relative to the bulk calculation. Both for tensile and for compressive strain, and for all methods, the P_0 values are much larger in the superlattice Ni-B than in bulk or than for the Ni A-site. This difference in P_0 is the quantum confinement effect: the barrier imposed by the AlO_2 layer has the effect of making the apical oxygen hybridize more strongly with the Ni B-site, thus raising the energy of the frontier antibonding Ni-O state and thereby depopulating the $3z^2 - r^2$ orbital. The effect is strongest in the GGA calculation, and is reduced as J is increased.

Turning now to the variation with octahedral distortion, we see that for tensile strain the fitted slope R is systematically smaller for the Ni-B site than for the Ni-A site or for the bulk calculation, and the actual data display a tendency to saturation. Conversely, for compressive strain the Ni B-site R is systematically larger than the A-site or bulk values. These observations indicate a strong coupling between quantum confinement and structural effects. For the B-site under tensile strain, the effect of the strain-induced decrease in apical Ni-O bond length is less significant because the O is already strongly bonded to the Ni and the quantum confinement effect is strong; this explains the decreased R value compared to the A-site or bulk. For compressive strain, the tendency to increase the Ni-O distance weakens the Ni-O bond making the quantum confinement effect less important and conversely the octahedral distortion effect more influential; these effects explains the larger R value under compressive strain.

VI. ANALYSIS: MANY-BODY EFFECTS

The effect of correlations on orbital polarization is contained in the real parts of the electron self energies. The self energy is a 2×2 matrix. In the DMFT approximation used here it is site-local and for a given Ni site it is approximately diagonal in the orbital basis aligned with the axes of the NiO_6 octahedron. In this basis it has two components, corresponding to the $d_{x^2-y^2}$ and $d_{3z^2-r^2}$ orbitals. In the GGA+DMFT approach used here the double counting term is orbital-independent, so the difference between the real parts of the two diagonal components of the self energy provides a many-body correction to the difference in bare energy levels. A positive sign of $\Sigma_{d_{3z^2-r^2}} - \Sigma_{d_{x^2-y^2}}$ means that many-body effects shift the $3z^2 - r^2$ level up in energy relative to the $x^2 - y^2$ level, thus increasing P. Fig. 9 presents the zero frequency limit of the self energy difference, for the superlattice and the bulk system.

Consider first the results for the bulk material. We see that the self energy difference is positive (acts to increase

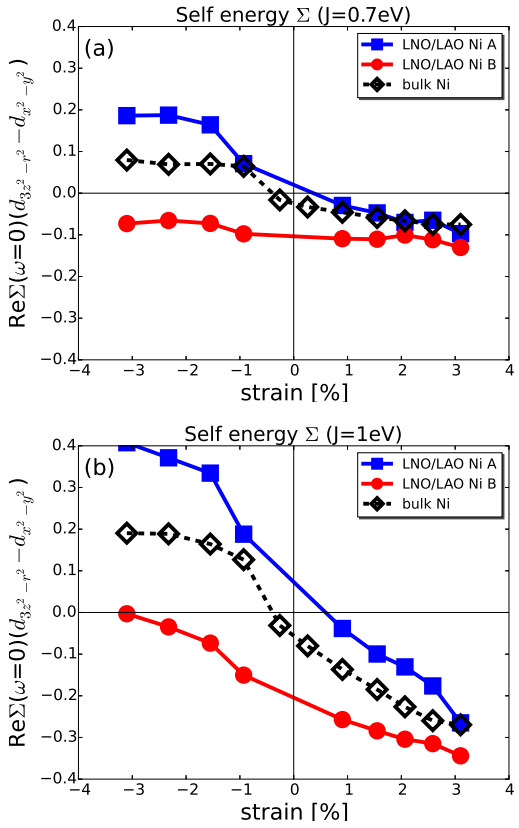

Figure 9. (Color online) The difference of the real part of the self energy $\Sigma_d(\omega = 0)$ between the $d_{3z^2-r^2}$ and the $d_{x^2-y^2}$ orbitals for the 4/4 $LaNiO_3/LaAlO_3$ superlattice (filled symbols and solid lines) and for strained bulk $LaNiO_3$ (open symbols and dashed line) for U=5eV and J-values of 0.7eV (panel a) and 1eV (panel b).

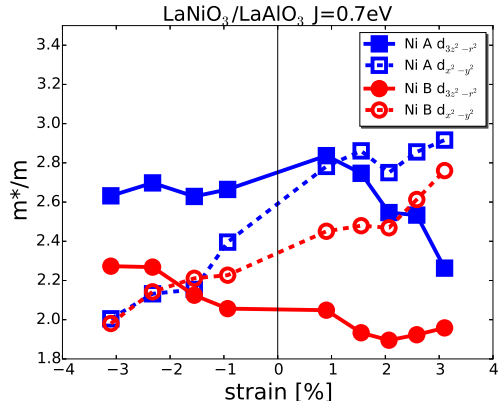

Figure 10. (Color online) The orbital-resolved mass enhancement m^*/m for the $d_{3z^2-r^2}$ (filled symbols) and the $d_{x^2-y^2}$ (open symbols) orbitals of the 4/4 $LaNiO_3/LaAlO_3$ superlattice as a function of strain (m^* is the effective mass of GGA+DMFT and m is the bare mass obtained within GGA). Both the inner Ni A (square and blue) and the outer Ni B (circular and red) layers are compared. U=5eV and J=0.7eV are used for GGA+DMFT calculations.

P) for compressive strain (except near zero strain where GGA P starts to change the sign) and negative (acts to decrease P) for tensile strain. We see that for both signs of strain, the magnitude of the self energy is twice as large for J = 1eV as it is for J = 0.7eV, and that the self energy has more strain dependence for tensile strain than for compressive strain. The difference in magnitude of the self energy Σ difference across $d = 0$ causes the decrease in P_0 between compressive and tensile strain. A dependence of the magnitude of $\delta\Sigma$ on strain provides the renormalization of R. We see that for the bulk material, the change of the magnitude of Σ is much larger than that of the $\delta\Sigma$ dependence on strain and this $\delta\Sigma$ dependence is larger for tensile than for compressive strain. These results explain the strong reduction of P_0 compared to R and the difference in renormalization of R reported above.

We now turn to the superlattice. We see that generically the sign of the self energy is such that the many-body effects act to drive the polarization towards zero for both Ni sites regardless of strain or quantum confinement. Thus for the B-site the self energy difference is always negative (decreases P) because quantum confinement effects produce positive GGA P values for all strain values. The Ni A self energy changes sign because the sign of P also changes. The sign change does not take place at exactly the same strain value in both quantities because P is determined by an average of $Re\Sigma$ over a range of frequencies.

The DMFT self energy also encodes the mass enhancement effect which can quantify the electronic correlation strength. We show in Fig. 10 the mass enhancement m^*/m for the 4/4 $LaNiO_3/LaAlO_3$ superlattices for the $d_{3z^2-r^2}$ (filled symbols) and the $d_{x^2-y^2}$ (open symbols) orbitals. For Ni A (square and blue dots) at large tensile strain, the $d_{3z^2-r^2}$ m^*/m decreases as the apical bond-length l_c becomes small while the $d_{x^2-y^2}$ m^*/m increases due to the large l_a. The change of the bond angle also affects m^*/m, however the trend under strain is opposite from that of the bond-length. For example, the $d_{3z^2-r^2}$ m^*/m in Ni A becomes larger across the zero strain as the bond angle α increases (see Fig. 8) even though l_c is decreasing toward the tensile strain. Similar effects of strain on m^*/m of the bulk $LaNiO_3$ have already been reported in Ref. 36. Ni B (circular and red) displays a similar m^*/m behavior for the $d_{x^2-y^2}$ orbital while the $d_{3z^2-r^2}$ m^*/m is quite reduced compared to the Ni A $d_{3z^2-r^2}$ orbital due to the enhanced hybridization effect of the Ni B $d_{3z^2-r^2}$ orbital.

To further confirm the consistent behavior of orbital polarization for the ultra-thin limit, we also computed the 1/1 $LaNiO_3/LaAlO_3$ superlattice (which should exhibit stronger quantum confinement effects since the Ni site is bounded on two sides by the insulator) at U=5eV and J=0.7eV for the most compressive strain (-3.1%) and the most tensile strain (3.1%). Under compressive strain, Ni P computed using GGA is -16.52% while GGA+DMFT produces P = 7.4%. The large offset and

the sign change are very similar to that seen in the B-site of the 4/4 superlattice, confirming that the effect is related to quantum confinement. Under tensile strain, GGA P is 23.63% and GGA+DMFT reduces the P value to 15.27%, a fractional reduction similar to that found for the B-site in the 4/4 superlattice, confirming that the quantum confinement effects are more important in this case.

VII. CONCLUSION

This paper presents a theoretical study of the layer-resolved orbital polarization of strained 4/4 $LaNiO_3/LaAlO_3$ perovskite superlattices. We used spin polarized GGA to obtain relaxed structures and paramagnetic GGA+DMFT to account for correlations on the Ni sites. Our calculations introduce two kinds of external symmetry breaking: c-axis quantum confinement associated with the insulating spacer layers and lattice strain. We further analyze these perturbations in terms of the resulting octahedral symmetry breaking caused by structural relaxations that lead to a difference between the apical (c-axis) Ni-O bond length l_c and the in-plane bond length l_a, as well as rotational and tilting distortions of NiO_6 octahedra. By comparing many-body and pure GGA calculations, as well as superlattice and strained bulk calculations, we are able to separate the effects.

The results presented here indicate that strain affects orbital polarization in two ways: it deforms the NiO_6 octahedra, thereby explicitly leading to a splitting of the two Ni e_g states, and it changes the type of octahedral rotation pattern observed for tensile versus compressive strain. It is useful to express the polarization as the sum of a term proportional to the octahedral distortion of a NiO_6 octahedron and a residual arising from quantum confinement and octahedral rotation effects (see Table I). While in strained bulk $LaNiO_3$ the change in rotation angles has only a small effect on orbital polarization, in the superlattice the effect is larger. We further find that proximity to the insulating AlO_2 layer has a dramatic effect on the polarization. This quantum confinement effect is at least as important as the strain effects, but is very local, affecting the outer-layer Ni B site substantially and the inner-layer Ni A site hardly at all. Finally, we note that quantum confinement and strain effects combine in interesting ways. For tensile strain the superlattice Ni B exhibits a reduced R value than bulk materials due to quantum confinement, while for compressive strain the R value for Ni B can be larger since the octahedral distortion effect on the change of P is more important.

Our calculations reproduce the experiment[7] semiquantitatively, yielding differences between the polarizations of the Ni A and B sites with about the correct order of magnitude and with a strain dependence of the correct order of magnitude. GGA+DMFT is clearly an improvement over pure GGA calculations. We demonstrate that the results have some sensitivity to the value of the on-site interaction J, and the optimal value to describe experiment lies somewhere between the values of 0.7 and 1.0 eV used in this study.

An important direction for future work is to extend the ideas introduced here to interfaces involving 'early' transition metal oxides such as the La and Sr titanates and vanadates. These materials are closer to the Mott/Hubbard limit (hybridization to oxygen less important and d-valence closer to formal valence), whereas the nickelates are in the 'negative charge transfer' limit (hybridization to oxygen crucial and d-occupancy much closer to d^8 than to the d^7 predicted by formal valence considerations. These differences suggest that the early transition metal oxides may be much more susceptible to orbital polarization effects than are the nickelates.

ACKNOWLEGEMENTS

We thank A. Georges and O. Peil for helpful discussions and pointing out an inaccuracy in the structural relaxation calculations in an earlier version of this paper. H. Park acknowledges support of the start-up funding from UIC and Argonne National Laboratory (by the US Department of Energy, Office of Science program). The work of AJM on this project was supported by the basic energy sciences program of the US Department of Energy under grant ER-046169. CAM and H. Park acknowledge support from FAME, one of six centers of STARnet, a Semiconductor Research Corporation program sponsored by MARCO and DARPA. We gratefully acknowledge the computing resources provided on Blues and/or Fusion, a high-performance computing cluster operated by the Laboratory Computing Resource Center at Argonne National Laboratory. We also acknowledge computational facilities provided via XSEDE resources through Grant No. TG-PHY130003. A.J.M. acknowledges the warm hospitality and stimulating intellectual environment of the College de France, where part of the writing of this manuscript was completed.

[1] M. Imada, A. Fujimori, and Y. Tokura, Rev. Mod. Phys. **70**, 1039 (1998).
[2] J. Chakhalian, J. W. Freeland, A. J. Millis, C. Panagopoulos, and J. M. Rondinelli, Rev. Mod. Phys. **86**, 1189 (2014).
[3] P. Zubko, S. Gariglio, M. Gabay, P. Ghosez, and J.-M. Triscone, Annual Review of Condensed Matter Physics **2**, 141 (2011).
[4] J. c. v. Chaloupka and G. Khaliullin, Phys. Rev. Lett. **100**, 016404 (2008).

[5] P. Hansmann, X. Yang, A. Toschi, G. Khaliullin, O. K. Andersen, and K. Held, Phys. Rev. Lett. **103**, 016401 (2009).

[6] M. J. Han, X. Wang, C. A. Marianetti, and A. J. Millis, Phys. Rev. Lett. **107**, 206804 (2011).

[7] M. Wu, E. Benckiser, M. W. Haverkort, A. Frano, Y. Lu, U. Nwankwo, S. Brück, P. Audehm, E. Goering, S. Macke, V. Hinkov, P. Wochner, G. Christiani, S. Heinze, G. Logvenov, H.-U. Habermeier, and B. Keimer, Phys. Rev. B **88**, 125124 (2013).

[8] J. Chakhalian, J. M. Rondinelli, J. Liu, B. A. Gray, M. Kareev, E. J. Moon, N. Prasai, J. L. Cohn, M. Varela, I. C. Tung, M. J. Bedzyk, S. G. Altendorf, F. Strigari, B. Dabrowski, L. H. Tjeng, P. J. Ryan, and J. W. Freeland, Phys. Rev. Lett. **107**, 116805 (2011).

[9] J. W. Freeland, J. Liu, M. Kareev, B. Gray, J. W. Kim, P. Ryan, R. Pentcheva, and J. Chakhalian, EPL (Europhysics Letters) **96**, 57004 (2011).

[10] P. Hansmann, A. Toschi, X. Yang, O. K. Andersen, and K. Held, Phys. Rev. B **82**, 235123 (2010).

[11] N. Parragh, G. Sangiovanni, P. Hansmann, S. Hummel, K. Held, and A. Toschi, Phys. Rev. B **88**, 195116 (2013).

[12] M. J. Han, C. A. Marianetti, and A. J. Millis, Phys. Rev. B **82**, 134408 (2010).

[13] O. E. Peil, M. Ferrero, and A. Georges, Phys. Rev. B **90**, 045128 (2014).

[14] H. Chen, D. P. Kumah, A. S. Disa, F. J. Walker, C. H. Ahn, and S. Ismail-Beigi, Phys. Rev. Lett. **110**, 186402 (2013).

[15] A. S. Disa, D. P. Kumah, A. Malashevich, H. Chen, D. A. Arena, E. D. Specht, S. Ismail-Beigi, F. J. Walker, and C. H. Ahn, Phys. Rev. Lett. **114**, 026801 (2015).

[16] H. Park, A. J. Millis, and C. A. Marianetti, Phys. Rev. B **90**, 235103 (2014).

[17] H. Park, A. J. Millis, and C. A. Marianetti, Phys. Rev. Lett. **109**, 156402 (2012).

[18] Z. He and A. J. Millis, Phys. Rev. B **91**, 195138 (2015).

[19] K. Momma and F. Izumi, Journal of Applied Crystallography **44**, 1272 (2011).

[20] G. Kresse and J. Furthmuller, Phys. Rev. B **54**, 11169 (1996).

[21] G. Kresse and D. Joubert, Phys. Rev. B **59**, 1758 (1999).

[22] P. E. Blöchl, Phys. Rev. B **50**, 17953 (1994).

[23] J. P. Perdew, K. Burke, and M. Ernzerhof, Phys. Rev. Lett. **77**, 3865 (1996).

[24] H. Park, A. J. Millis, and C. A. Marianetti, Phys. Rev. B **89**, 245133 (2014).

[25] A. M. Glazer, Acta Crystallographica Section B **28**, 3384 (1972).

[26] A. M. Glazer, Acta Crystallographica Section A **31**, 756 (1975).

[27] J. L. García-Muñoz, J. Rodríguez-Carvajal, P. Lacorre, and J. B. Torrance, Phys. Rev. B **46**, 4414 (1992).

[28] J. A. Alonso, M. J. Martínez-Lope, M. T. Casais, J. L. García-Muñoz, M. T. Fernández-Díaz, and M. A. G. Aranda, Phys. Rev. B **64**, 094102 (2001).

[29] A. V. Boris, Y. Matiks, E. Benckiser, A. Frano, P. Popovich, V. Hinkov, P. Wochner, M. Castro-Colin, E. Detemple, V. K. Malik, C. Bernhard, T. Prokscha, A. Suter, Z. Salman, E. Morenzoni, G. Cristiani, H.-U. Habermeier, and B. Keimer, Science **332**, 937 (2011).

[30] A. Frano, E. Schierle, M. W. Haverkort, Y. Lu, M. Wu, S. Blanco-Canosa, U. Nwankwo, A. V. Boris, P. Wochner, G. Cristiani, H. U. Habermeier, G. Logvenov, V. Hinkov, E. Benckiser, E. Weschke, and B. Keimer, Phys. Rev. Lett. **111**, 106804 (2013).

[31] A. A. Mostofi, J. R. Yates, Y.-S. Lee, I. Souza, D. Vanderbilt, and N. Marzari, Computer Physics Communications **178**, 685 (2008).

[32] P. Werner and A. J. Millis, Phys. Rev. B **74**, 155107 (2006).

[33] K. Haule, Phys. Rev. B **75**, 155113 (2007).

[34] S. J. May, J.-W. Kim, J. M. Rondinelli, E. Karapetrova, N. A. Spaldin, A. Bhattacharya, and P. J. Ryan, Phys. Rev. B **82**, 014110 (2010).

[35] M. K. Kinyanjui, Y. Lu, N. Gauquelin, M. Wu, A. Frano, P. Wochner, M. Reehuis, G. Christiani, G. Logvenov, H.-U. Habermeier, G. A. Botton, U. Kaiser, B. Keimer, and E. Benckiser, Applied Physics Letters **104**, 221909 (2014).

[36] E. A. Nowadnick, J. P. Ruf, H. Park, P. D. C. King, D. G. Schlom, K. M. Shen, and A. J. Millis, Phys. Rev. B **92**, 245109 (2015).